

Photoplethysmograph Signal Reconstruction based on a Novel Motion Artifact Detection-Reduction Approach. Part II: Motion and Noise Artifact Removal

S. M. A. SALEHIZADEH,¹ DUY K. DAO,¹ JO WOON CHONG,¹ DAVID MCMANUS,² CHAD DARLING,³
YITZHAK MENDELSON,¹ and KI H. CHON¹

¹Department of Biomedical Engineering, Worcester Polytechnic Institute, Worcester, MA 01609-2280, USA; ²Cardiology Division, Departments of Medicine and Quantitative Health Sciences, University of Massachusetts Medical Center, Worcester, MA 01655, USA; and ³Department of Emergency Medicine, University of Massachusetts Medical School, Worcester, MA 01655, USA

(Received 28 February 2014; accepted 6 May 2014; published online 14 May 2014)

Associate Editor Tingrui Pan oversaw the review of this article.

Abstract—We introduce a new method to reconstruct motion and noise artifact (MNA) contaminated photoplethysmogram (PPG) data. A method to detect MNA corrupted data is provided in a companion paper. Our reconstruction algorithm is based on an iterative motion artifact removal (IMAR) approach, which utilizes the singular spectral analysis algorithm to remove MNA artifacts so that the most accurate estimates of uncorrupted heart rates (HRs) and arterial oxygen saturation (SpO₂) values recorded by a pulse oximeter can be derived. Using both computer simulations and three different experimental data sets, we show that the proposed IMAR approach can reliably reconstruct MNA corrupted data segments, as the estimated HR and SpO₂ values do not significantly deviate from the uncorrupted reference measurements. Comparison of the accuracy of reconstruction of the MNA corrupted data segments between our IMAR approach and the time-domain independent component analysis (TD-ICA) is made for all data sets as the latter method has been shown to provide good performance. For simulated data, there were no significant differences in the reconstructed HR and SpO₂ values starting from 10 dB down to −15 dB for both white and colored noise contaminated PPG data using IMAR; for TD-ICA, significant differences were observed starting at 10 dB. Two experimental PPG data sets were created with contrived MNA by having subjects perform random forehead and rapid side-to-side finger movements show that; the performance of the IMAR approach on these data sets was quite accurate as non-significant differences in the reconstructed HR and SpO₂ were found compared to non-contaminated reference values, in most subjects. In comparison, the accuracy of the TD-ICA was poor as there were significant

differences in reconstructed HR and SpO₂ values in most subjects. For non-contrived MNA corrupted PPG data, which were collected with subjects performing walking and stair climbing tasks, the IMAR significantly outperformed TD-ICA as the former method provided HR and SpO₂ values that were non-significantly different than MNA free reference values.

Keywords—Motion artifact removal, Blind source separation, Singular spectrum analysis.

INTRODUCTION

Arterial oxygen saturation reflects the relative amount of oxyhemoglobin in the blood. The most common method to measure it is based on pulse oximetry, whereby oxidized hemoglobin and reduced hemoglobin have significantly different optical spectra. Specifically, at a wavelength of about 660 nm, and a second wavelength between 805 and 960, there is a large difference in light absorbance between reduced and oxidized hemoglobin. A measurement of the percent oxygen saturation of blood is defined as the ratio of oxyhemoglobin to the total concentration of hemoglobin present in the blood. Pulse oximetry assumes that the attenuation of light is due to both the blood and bloodless tissue. Fluctuations of the PPG signal are caused by changes in arterial blood volume associated with each heartbeat, where the magnitude of the fluctuations depends on the amount of blood rushing into the peripheral vascular bed, the optical absorption of the blood, skin, and tissue, and the wavelength used to illuminate the blood.

Address correspondence to Ki H. Chon, Department of Biomedical Engineering, Worcester Polytechnic Institute, Worcester, MA 01609-2280, USA. Electronic mail: ssalehizadeh@wpi.edu, dkdao@wpi.edu, jchong@wpi.edu, mcmansud@ummc.org, Chad.Darling@umassmed.edu, ym@wpi.edu, kichon@wpi.edu

The pulse oximeter signal contains not only the blood oxygen saturation and heart rate (HR) data, but also other vital physiological information. The fluctuations of photoplethysmogram (PPG) signals contain the influences of arterial, venous, autonomic and respiratory systems on the peripheral circulation. In the current environment where health care costs are ever increasing, a single sensor that has multiple functions is very attractive from a financial perspective. Moreover, utilizing a pulse oximeter as a multi-purpose vital sign monitor has clinical appeal, since it is familiar to the clinician and comfortable for the patient. Knowledge of respiratory rate³ and HR patterns would provide more useful clinical information in many situations in which pulse oximeter is the sole monitor available.

Although there are many promising and attractive features of using pulse oximeters for vital sign monitoring, currently they are used on stationary patients. This is mainly because motion and noise artifacts (MNAs) result in unreliable HR and SpO₂ estimation. Clinicians have cited motion artifacts in pulse oximetry as the most common cause of false alarms, loss of signal, and inaccurate readings.¹⁴ A smart watch with a PPG sensor is currently commercially available for monitoring HRs (www.mioglobal.com). However, MNA is a big source of problem for accurate vital extraction from PPG signals and prevents wide adoption of this potentially useful technology for mobile health.

In practice MNA are difficult to remove because they do not have a predefined narrow frequency band and their spectrum often overlaps that of the desired signal.²⁷ Consequently, development of algorithms capable of reconstructing the corrupted signal and removing artifacts is challenging.

There are a number of general techniques used for artifact detection and removal. One of the methods used to remove motion artifacts is adaptive filtering.^{1,5,15,19,24} An adaptive filter is easy to implement and it also can be used in real-time applications, though the requirement of additional sensors to provide reference inputs is the major drawback of such methods.

There are many MNA reduction techniques based on the concept of blind source separation (BSS). BSS is attractive and has garnered significant interest since this approach does not require a reference signal. The aim of the BSS is to estimate a set of uncorrupted signals from a set of mixed signals which is assumed to contain both the clean and MNA sources.² Some of the popular BSS techniques are independent component analysis (ICA),⁴ canonical correlation analysis (CCA),²⁸ principle component analysis (PCA),¹³ and singular spectrum analysis (SSA).⁶

In ICA, the recorded signals are decomposed into their independent components or sources.⁴ CCA uses the second order statistics to generate components

derived from their uncorrelated nature.⁸ PCA is another noise reduction technique which aims to separate the clean signal dynamics from the MNA data. A multi-scale PCA has been also proposed to account for time-varying dynamics of the signal and motion artifacts from PPG recordings.²⁰

A promising approach that can be applied to signal reconstruction is the SSA. The SSA is a model-free BSS technique, which decomposes the data into a number of components which may include trends, oscillatory components, and noise (see historical reviews in Ref. 10). The main advantage of SSA over ICA is that SSA does not require user input to choose the appropriate components for reconstruction and MNA removal. Comparing PCA to SSA, SSA can be applied in cases where the number of signal components is more than the rank of the PCA covariance matrix. Applications of the SSA include extraction of the amplitude and low frequency artifacts from single channel EEG recordings,²⁶ and removing heart sound dynamics from respiratory signals.⁹

In this paper, we introduce a novel approach to reconstruct a PPG signal from those portions of data that have been identified to be corrupted using the algorithm detailed in Part I of the companion paper. The fidelity of the reconstructed signal was determined by comparing the estimated SpO₂ and HR to reference values. In addition, we compare the reconstructed SpO₂ and HR values obtained *via* the time-domain ICA (TD-ICA) to our method. We have chosen to compare our method to TD-ICA since the latter has recently been shown to provide good reconstruction of corrupted PPG signals.¹⁸

MATERIALS AND METHOD

Experimental Protocol and Preprocessing

Three sets of data were collected from healthy subjects recruited from the student community of Worcester Polytechnic Institute (WPI). This study was approved by WPI's institutional review board and all the subjects gave informed consent before data recording.

In the first experiment, 11 healthy volunteers were asked to wear a forehead reflectance pulse oximeter developed in our lab along with a reference Masimo Radical (Masimo SET[®]) finger transmittance pulse oximeter. PPG signals from the forehead sensor and reference (HR) derived from a finger pulse oximeter were acquired simultaneously. The HR and SpO₂ signals were acquired at 80 and 1 Hz, respectively. After baseline recording for 5 min without any movement (i.e., clean data), motion artifacts were induced in the PPG data by the spontaneous movements in both

horizontal and vertical directions of the subject's head while the right middle finger was kept stationary. Subjects were directed to introduce the motions for specific time intervals that determined the percentage of noise within each 1 min segment, varying from 10 to 50%. For example, if a subject was instructed to make left-right movements for 6 s, an 1 min segment of data would contain 10% noise. Note that noise amplitudes varied among subjects due to their head movements.

The second dataset consisted of finger-PPG signals from the nine healthy volunteers in an upright sitting posture using an infrared reflection type PPG transducer (TSD200). An MP1000 pulse oximeter (BIOPAC Systems Inc., CA, USA) was also used to acquire finger PPG signals at 100 Hz. One pulse oximeter of each model was placed on the same hand's index finger (one model) and middle finger (the other model) simultaneously. After baseline recording for 5 min without any movement (i.e., clean data), motion artifacts were induced in the PPG data by the left-right movements of the index finger while the middle finger was kept stationary to provide a reference. This was accomplished by placing the middle finger on top of the edge of a table while the index finger moved in the free space off the edge of the table. Similar to the first dataset, motion was induced at specific time intervals corresponding to 10–50% corruption duration in 1 min segments, i.e., the controlled movement was carried out five times per subject.

The third dataset consisted of data measurements from nine subjects with the PPG signal recorded from the subjects' foreheads using our custom sensor (80 Hz) simultaneously with the reference ECG from a Holter Monitor at 180 Hz and reference HR and SpO₂ derived from a Masimo (Rad-57) pulse oximeter at 0.5 Hz, respectively. The reference pulse oximeter provided HR and SpO₂ measured from the subject's right index finger, which was held steadily to their chest. The signals were recorded while the subjects were going through sets of walking and climbing up and down flights of stairs for approximately 45 min.

Once data were acquired, PPG signals from all three experiments outlined above were preprocessed offline using Matlab (MathWorks, R2012a). The PPG signals were filtered using a zero-phase forward-reverse 4th order IIR band-pass filter with cutoff frequency 0.5-12 Hz.

MOTION ARTIFACT REMOVAL

To reconstruct the artifact-corrupted portion of the PPG signal that has been detected using the support vector machine approach provided in the accompanying paper, we propose a novel hybrid procedure using Iterative Singular Spectrum Analysis (ISSA) and

a frequency matching algorithm. Henceforth, we will call these combined procedures the iterative motion artifact removal (IMAR) algorithm.

SINGULAR SPECTRUM ANALYSIS

The SSA is composed of two stages: singular decomposition and spectral reconstruction. The former is the spectral decomposition or eigen-decomposition of the data matrix whereas the latter is the reconstruction of the signal based on using only the significant eigenvectors and associated eigenvalues. The assumption is that given a relatively high signal-to-noise ratio of data, significant eigenvectors and associated eigenvalues represent the signal dynamics and less significant values represent the MNA components.

The calculation of the singular stage of the SSA consists of two steps: embedding followed by singular value decomposition (SVD). In essence, these procedures decompose the data into signal dynamics consisting of trends, oscillatory components, and MNA. The spectral stage of the SSA algorithm also consists of two steps: grouping and diagonal averaging. These two procedures are used to reconstruct the signal dynamics but without the MNA components. In the following section, we detail all four steps in the SSA algorithm.

Singular Decomposition

Embedding

Assume we have a nonzero real-value time series of length N samples, i.e., $X = \{x_1, x_2, \dots, x_N\}$. In the embedding step, window length $f_s/f_l < L < N/2$ is chosen to embed the initial time series, where f_s is the sampling frequency and f_l is the lowest frequency in the signal. We map the time series X into the L lagged vectors, $X = \{x_i, x_{i+1}, \dots, x_{i+L-1}\}$ for $i = 1, \dots, K$, where $K = N - L + 1$.¹⁰ The result is the trajectory data matrix T_x or vector X_i that is each row of T_x for $i = 1, \dots, K$.

$$T_x = \begin{bmatrix} X_1 \\ X_2 \\ \vdots \\ X_K \end{bmatrix} = \begin{bmatrix} x_1 & x_2 & \cdots & x_L \\ x_2 & x_3 & \cdots & x_{L+1} \\ \vdots & \vdots & \ddots & \vdots \\ x_K & x_{K+1} & \cdots & x_N \end{bmatrix} \quad (1)$$

From Eq. (1), it is evident that the trajectory matrix, T_x , is a Hankel matrix.

Singular Value Decomposition

The next step is to apply the SVD to the trajectory matrix T_x which results in eigenvalues and eigenvectors

of the matrix $T_x T_x^T$ where T_i for $i = 1, \dots, L$ can be defined as $T = USV^T$.¹⁰ U_i for $1 < i < L$ is a $K \times L$ orthonormal matrix. S_i for $1 < i < L$ is a diagonal matrix and V_i for $1 < i < L$ is an $L \times L$ square orthonormal matrix, which is considered the principle component. In this step, T_x has L many singular values which are $\sqrt{\lambda_1} > \sqrt{\lambda_2} > \dots, \sqrt{\lambda_L}$. By removing components with eigenvalues equal to zero, the i th eigentriple of T_i can be written as $U_i \times \sqrt{\lambda_i} \times V_i^T$ for $i = 1, 2, \dots, d$, in which $d = \max(i : \sqrt{\lambda_i} > 0)$ is the number of nonzero singular values of T_x . Normally every harmonic component with a different frequency produces two eigentriples with similar singular values. So the trajectory matrix T_x can be denoted as¹⁰

$$\begin{aligned} T_x &= T_1 + T_2 + \dots + T_d \\ &= U_1 \sqrt{\lambda_1} V_1^T + \dots + U_d \sqrt{\lambda_d} V_d^T \\ &= \sum_{i=1}^d U_i \sqrt{\lambda_i} V_i^T \end{aligned} \quad (2)$$

Projecting the time series onto the direction of each eigenvector yields the corresponding temporal principal component (PC).⁷

Spectral Reconstruction

The reconstruction stage has two steps: grouping and diagonal averaging. First the subgroups of the decomposed trajectory matrices are grouped and then a diagonal averaging step is needed so that a new time series can be formed.⁶

Grouping

The grouping step of the reconstruction stage decomposes the $L \times K$ matrix T_i ($i = 1, 2, \dots, d$) into subgroups according to the trend, oscillatory components, and MNA dynamics. The grouping step divides the set of indices $\{1, 2, \dots, d\}$ into a collection of m disjoint subsets of $I = \{I_1, \dots, I_m\}$.¹² Thus, T_I corresponds to the group $I = \{I_1, \dots, I_m\}$. T_I is a sum of T_j , where $j \in I_i$. So T_x can be expanded as

$$T_x = \overbrace{T_1 + \dots + T_L}^{SVD} = \overbrace{T_{I_1} + \dots + T_{I_m}}^{\text{Grouping}} \quad (3)$$

Diagonal Averaging

In the final step of analysis, each resultant matrix, T_{I_i} , in Eq. (3) is transformed into a time series of length N . We obtain the new Hankel matrices $\tilde{X}^{(i)}$ by averaging the diagonal elements of the matrix T_{I_i} .⁷ Let H be denoted as the Hankel operator. So that we obtain the Hankel matrix $\tilde{X}^{(i)} = HT_{I_i}$ for $i = 1, \dots, m$.¹² Under the assumption of weak separa-

bility and applying the Hankel procedure to all matrix components of Eq. (3), we obtain the following expansion

$$X = \tilde{X}^{(1)} + \tilde{X}^{(2)} + \dots + \tilde{X}^{(M)} \quad (4)$$

We can assert that $\tilde{X}^{(1)}$ is related to the trend of the signal; however, harmonic and noisy components do not necessarily follow the order of $\sqrt{\lambda_1} > \sqrt{\lambda_2} > \dots > \sqrt{\lambda_M}$.

ITERATIVE MOTION ARTIFACT REMOVAL BASED ON SSA

In order to reconstruct the MNA corrupted segment of the signal, an IMAR approach based on SSA was explained in the last section. The ultimate goodness of the reconstructed signal is determined by the accuracy of the estimated SpO₂ and HR values. The top and bottom panels of Fig. 1 show clean and MNA corrupted signals, respectively. The most important part of the SSA is to choose the proper eigenvector components for reconstruction of the signal. Under the assumption of high SNR, the normal practice is to select only the largest eigenvalues and associated eigenvectors for signal reconstruction. However, most often it is difficult to determine the demarcation of the significant from non-significant eigenvalues. Further, the MNA dynamics can overlap with the signal dynamics, hence, choosing the largest eigenvalues does not necessarily result in an MNA-free signal.

To overcome the above limitations, we have modified the SSA approach. The first step of our modified SSA involves computing SVD on both a corrupted data segment and its most prior adjacent clean data segment. Under the assumption of a high SNR of the data, the second step is to retain only the top 5% of the eigenvalues and their associated eigenvectors. The third step is to replace the corrupted segment's top 5% eigenvalues with the clean segment's eigenvalues. The fourth step is to further limit the number of eigenvectors by choosing only those eigenvectors that have HRs between $0.66 \text{ Hz} < f_s < 3 \text{ Hz}$ for both the clean and noise corrupted data segments. The two extreme HRs are chosen so that they account for possible scenarios that one may encounter with low and high HRs. With the remaining candidate eigenvectors resulting from step four, we further prune non-significant eigenvectors by performing frequency matching of the noise corrupted eigenvectors to those of the clean data segment's eigenvectors, in the fifth step. Only those eigenvectors' frequencies that match to those of the clean eigenvectors are retained from the pool of eigenvectors remaining from step four. For the remaining eigenvector candidates, we perform iterative

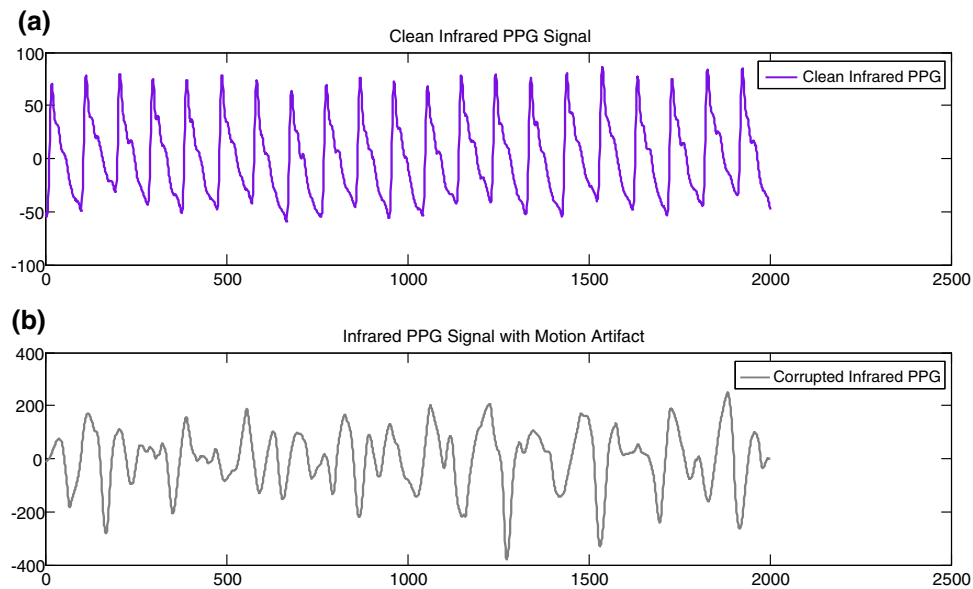


FIGURE 1. Typical infrared PPG signal; (a) clean, (b) corrupted with motion artifacts.

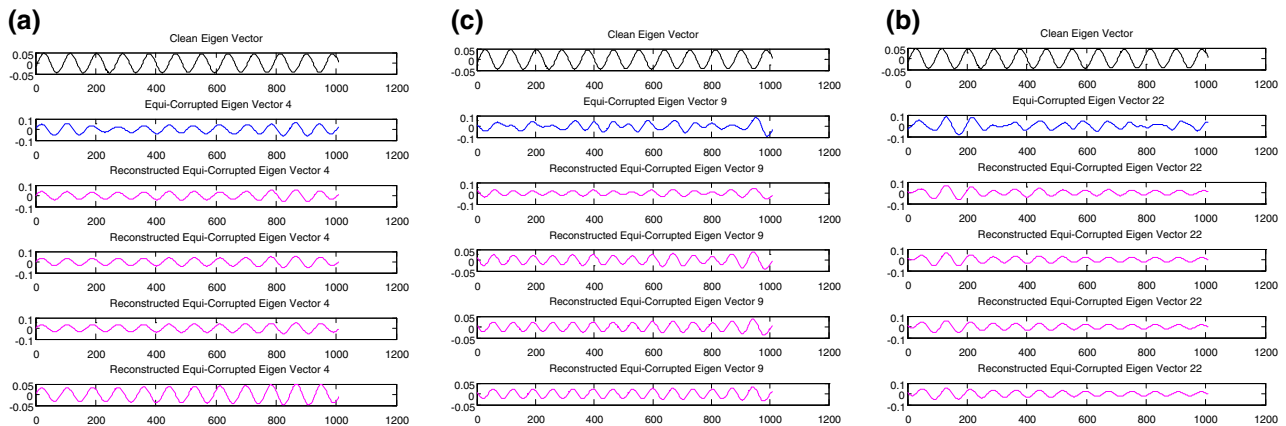


FIGURE 2. Iterative reconstruction of a corrupted eigenvector with frequency of 0.967 Hz. Black font signals (top panels) represent the clean component with frequency of 0.967 Hz; Blue font signals (2nd rows) indicate the corrupted component with the same frequency; Pink font signals are related to iterative evolution of corrupted component to a clean oscillatory signal. (a) Reconstruction of 4th corrupted eigenvector compared to the corresponding clean component. The final pattern after 4 iterations resembles the black font clean component in the top panel. This component is chosen among the components with the same frequency, since it shows the most similarity to the black font clean component. (b) Reconstruction of 9th corrupted eigenvector compared to the corresponding clean component. (c) Reconstruction of 22nd corrupted eigenvector compared to the corresponding clean component.

SSA to further reduce MNA and match the dynamics of the clean data segments' eigenvectors for the final step. For each iteration we perform the standard SSA algorithm. It is our experience that this convergence is achieved within 4 iterations.

Figure 2 shows an example of the iterative SSA procedure applied to candidate eigenvectors that have resulted from step four of the procedure for the modified SSA algorithm. Note that there may be several eigenvectors remaining after the fifth step, hence, this example shows an iterative SSA procedure performed on a particular set of candidate eigenvectors that may

match most closely to an eigenvector of a clean data segment. The top row of panels of Fig. 2 represents one of the eigenvectors of the clean signal and the second row of panels represents the MNA corrupted signal's candidate eigenvectors which have the same frequency as that of the clean signal's eigenvector. The remaining lower panels of Fig. 2 represent the candidate eigenvectors after they have gone through four successive iterations of the SSA algorithm. For this portion of the SSA algorithm, we perform SVD on the trajectory matrix of Eq. (1) created from the candidate eigenvector and then reconstruct the eigenvectors

TABLE 1. Iterative motion artifact removal (IMAR) procedure.

Assumption—Heart rate and SpO₂ do not change abruptly and are stationary within the short data segment
Application—Offline Motion Artifact Removal
Objective—Reconstruction of corrupted PPG segment for the purpose of estimating heart rates and SpO₂

 Routine

- Step 1.* First, compute SVD on both corrupted data segments and their most prior adjacent clean data segments
Step 2. Next, keep the top 5% of the clean and corrupted components, based on the eigenvalues being sorted from largest to smallest
Step 3. Replace the corrupted eigenvalues with corresponding clean eigenvalues
Step 4. Among the clean and corrupted components, only choose those with frequency within the heart rate frequency range of $0.66 < F_s < 3$ Hz
Step 5. Apply frequency matching to discard those corrupted components (from Step 4) with different frequencies compared to clean components' frequencies
Step 6. Remove corruption from each component obtained from Step 5 by applying the basic SSA algorithm iteratively
 6.a. Calculate the discarding metric for components achieved from SSA iterations and their counterpart clean components from Eq. (5)
 6.b. Select those processed components with the closest DM and frequency value to the corresponding clean component's DM and frequency value
Step 7. Finally, reconstruct the corrupted PPG segment based on the components achieved from Step 6
-

based on SSA using only the first 3 largest eigenvalues obtained from the SVD. This process repeats iteratively until the shape of the reconstructed eigenvector closely resembles one of the clean eigenvectors with the same frequency. It can be seen from Fig. 2 that after 4 iterations the result shown in the (a) panel corresponds most closely to the clean signal's eigenvector, hence, this eigenvector is selected rather than the eigenvectors shown in panels b–c. We calculate the discarding metric (DM) at each iteration and compare this value to the DM value of the corresponding clean component. The DM is calculated according to:

$$DM = \sum |u| / L(u) \quad (5)$$

where u is the signal component, and $|\cdot|$, $L(\cdot)$ are absolute operator and component length, respectively. The entire procedure for the modified SSA algorithm is summarized in Table 1.

RESULTS

Noise Sensitivity Analysis

To validate the proposed IMAR procedure, we added different SNR levels of Gaussian white noise (GWN) and colored noise to an experimentally collected clean segment of PPG signal. The purpose of the simulation was to quantitatively determine the level of noise that can be tolerated by the algorithm. Seven different SNR levels ranging from 10 dB to –25 dB were considered. For each SNR level, 50 independent realizations of GWN and colored noise were added separately to a clean PPG signal. The Euler–Maruyama method was used to generate colored noise.¹⁷

Figure 3 shows the results of these simulations with additive GWN. The left panels show pre- and

post-reconstruction HR in comparison to the reference HR; the right panels show the corresponding comparison for SpO₂. Tables 2 and 3 show the mean and standard deviation values of the pre- (2nd column) and post-reconstruction (4th column), and the reference (3rd column) HR and SpO₂ values, respectively, for all SNR. The last columns of Tables 2 and 3 also show the estimated HR and SpO₂ values obtained by the TD-ICA method.¹⁸ As shown in Fig. 3 and Tables 2 and 3, the reconstructed HR and SpO₂ values using our IMAR approach were found to be not statistically different when compared to the reference values for all SNR except for –20 and –25 dB. However, the TD-ICA method fails and we obtain significantly different values to those of the reference HR and SpO₂ values when the SNR is lower than –10 dB.

Tables 4 and 5 show corresponding results to that of Tables 2 and 3 but with additive colored noise. Similar to the GWN case, the reconstructed HR and SpO₂ values using the proposed IMAR approach are found to be not significantly different than the reference values for all SNR except for –20 and –25 dB. Moreover, the TD-ICA compares poorly compared to our IMAR as the HR and SpO₂ values from the former method are found to be significantly different to the reference values for all SNR.

Heart Rate and SpO₂ Estimation from Forehead Sensor

As described in “[Motion Artifact Removal](#)” section, we collected PPG data under three different experimental settings so that our proposed approach could be more thoroughly tested and validated. For all three experimental settings, the efficacy of our IMAR approach for the reconstruction of the MNA-affected portion of the signal will be compared with the

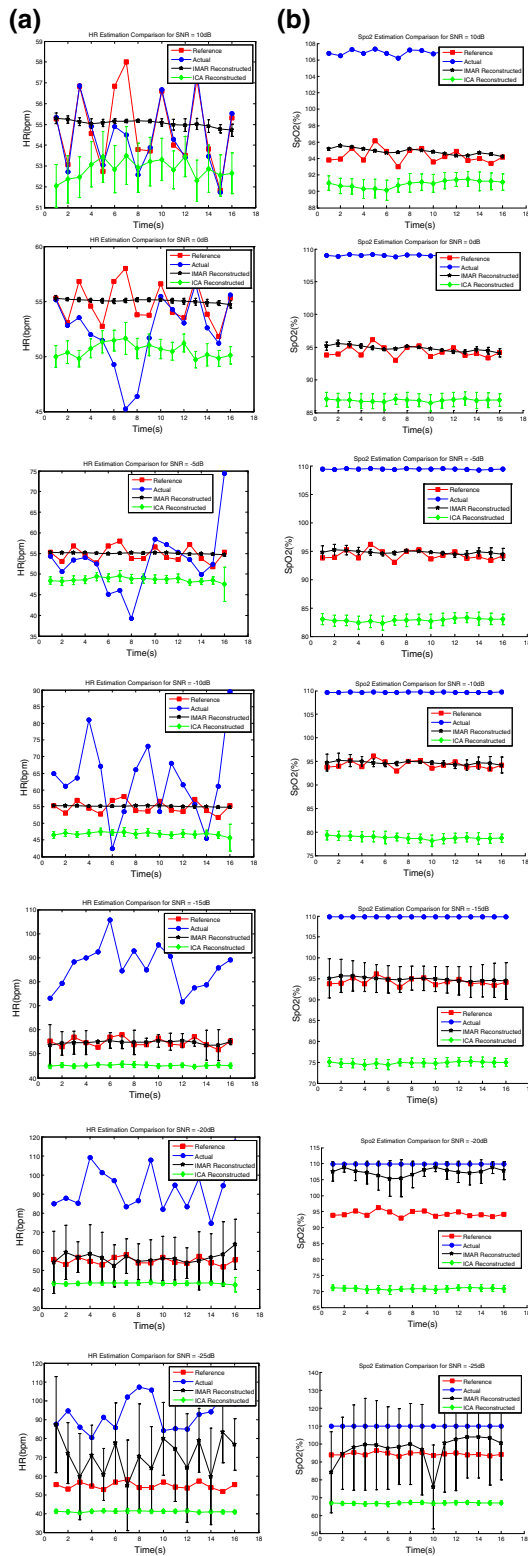


FIGURE 3. (Left) HR estimated from reconstructed PPG for different additive white noise levels; (Right) SpO₂ estimated from reconstructed PPG for different levels of additive white noise.

reference HR and SpO₂ values for all experimental datasets. Unlike Masimo's finger pulse oximeter, our custom-designed forehead pulse oximeter does not calculate moving average HR and SpO₂ values. This is the reason why the standard deviations of HR and SpO₂ values from the forehead sensor are much larger than those from Masimo's finger pulse oximeter (see Tables 6, 7, 8, 9, 10).

For the error-free SpO₂ estimation, Red and IR PPG signals with clearly separable DC and AC components are required. The pulsatile components of the Red and IR PPG signals are denoted as AC_{Red} and DC_{Red}, respectively, and the "ratio-of-ratio" R is estimated^{22,23} as

$$R = \frac{AC_{Red}/DC_{Red}}{AC_{IR}/DC_{IR}} \quad (6)$$

Accordingly, SpO₂ is computed by substituting the R value in an empirical linear approximate relation given by

$$SpO_2(\%) = (110 - 25R)(\%) \quad (7)$$

After applying the proposed IMAR procedure to the identified MNA segment of the PPG signal, we estimate the SpO₂ (using Eq. (6, 7)) and HR, and compare it to the corresponding reference and MNA contaminated segment values. As was the case with the "Noise Sensitivity Analysis" section, we compare the performance of the IMAR algorithm to the TD-ICA method. The top and bottom panels of Fig. 4 represent a representative HR and SpO₂ comparison result, respectively. We can see from these figures that the estimated values for both HR (left panels) and SpO₂ (right panels) from the IMAR (black font) track closely to the reference values recorded by the Masimo transmittance type finger pulse oximeter (red square line), while the estimated HR and SpO₂ obtained from the TD-ICA method (green font) deviate significantly from the reference signal. Tables 6 and 7 show comparison of the IMAR and the TD-ICA reconstructed HR and SpO₂ values, respectively, for all 10 subjects. As shown in Table 6, there was no significant difference between the finger reference HR and the IMAR reconstructed HR in 6 out of 10 subjects. However, there was significant difference between the finger reference HR and the TD-ICA reconstructed HR in all 10 subjects. Similarly, the reconstructed SpO₂ values from the IMAR were found to be not significantly different than the finger reference values in 6 out of 10 subjects, but the TD-ICA method was found to be significantly different for all 10 subjects.

TABLE 2. Comparison and statistical analysis of HR estimations from IMAR-reconstructed PPG for different levels of additive white noise.

SNR (dB)	Head HR (mean \pm SD)	Finger HR (Reference) (mean \pm SD)	IMAR reconstructed HR (mean \pm SD)	ICA reconstructed HR (mean \pm SD)
10	54.80 \pm 2.08	54.81 \pm 1.81	55.05 \pm 0.15	52.86 \pm 0.44*
0	54.80 \pm 2.72	54.81 \pm 1.81	55.05 \pm 0.14	50.58 \pm 0.62*
-5	56.37 \pm 8.18	54.81 \pm 1.81	55.05 \pm 0.15	48.64 \pm 0.51*
-10	46.02 \pm 22.93	54.81 \pm 1.81	55.09 \pm 0.15	46.85 \pm 0.45*
-15	121.62 \pm 69.33	54.81 \pm 1.81	54.73 \pm 0.62	45.17 \pm 0.28*
-20	80.08 \pm 37.69	54.81 \pm 1.81	56.49 \pm 2.69	43.08 \pm 0.32*
-25	103.62 \pm 52.49	54.81 \pm 1.81	76.45 \pm 7.52*	41.11 \pm 0.30*

* $p < 0.05$.**TABLE 3. Comparison & statistical analysis of estimations from IMAR-reconstructed PPG for different levels of additive white noise.**

SNR (dB)	Head SpO ₂ (mean \pm SD)	Finger SpO ₂ (Reference) (mean \pm SD)	IMAR reconstructed SpO ₂ (mean \pm SD)	ICA reconstructed SpO ₂ (mean \pm SD)
10	106.88 \pm 0.51	94.23 \pm 0.80	94.83 \pm 0.38	90.92 \pm 0.38*
0	108.98 \pm 0.14	94.23 \pm 0.80	94.81 \pm 0.42	86.88 \pm 0.16*
-5	109.42 \pm 0.06	94.23 \pm 0.80	94.77 \pm 0.26	82.86 \pm 0.27*
-10	109.69 \pm 0.04	94.23 \pm 0.80	94.68 \pm 0.30	78.81 \pm 0.29*
-15	109.82 \pm 0.02	94.23 \pm 0.80	94.90 \pm 0.41	74.88 \pm 0.23*
-20	109.89 \pm 0.01	94.23 \pm 0.80	107.38 \pm 1.06*	70.87 \pm 0.22*
-25	109.94 \pm 0.00	94.23 \pm 0.80	97.38 \pm 7.39*	66.91 \pm 0.26*

* $p < 0.05$.**TABLE 4. Comparison and statistical analysis of HR estimations from IMAR-reconstructed PPG for different levels of additive colored noise.**

SNR (dB)	Head HR (mean \pm SD)	Finger HR (Reference) (mean \pm SD)	IMAR reconstructed HR (mean \pm SD)	ICA reconstructed HR (mean \pm SD)
10	54.75 \pm 1.73	54.81 \pm 1.81	55.05 \pm 0.26	53.36 \pm 0.79
0	55.64 \pm 2.72	54.81 \pm 1.81	55.06 \pm 0.27	50.83 \pm 0.54*
-5	55.67 \pm 2.88	54.81 \pm 1.81	55.06 \pm 0.15	48.90 \pm 0.32*
-10	51.05 \pm 8.24	54.81 \pm 1.81	55.07 \pm 0.13	46.79 \pm 0.30*
-15	61.65 \pm 32.08	54.81 \pm 1.81	55.17 \pm 0.08	45.15 \pm 0.30*
-20	73.41 \pm 47.73	54.81 \pm 1.81	45.96 \pm 5.59*	42.96 \pm 0.41*
-25	66.37 \pm 40.80	54.81 \pm 1.81	61.86 \pm 2.12*	41.04 \pm 0.37*

* $p < 0.05$.**TABLE 5. Comparison and statistical analysis of SpO₂ estimations from IMAR-reconstructed PPG for different levels of additive colored noise.**

SNR (dB)	Head SpO ₂ (mean \pm SD)	Finger SpO ₂ (Reference) (mean \pm SD)	IMAR reconstructed SpO ₂ (mean \pm SD)	ICA reconstructed SpO ₂ (mean \pm SD)
10	94.14 \pm 0.99	94.23 \pm 0.80	94.85 \pm 0.41	90.95 \pm 0.18*
0	94.71 \pm 1.20	94.23 \pm 0.80	94.85 \pm 0.53	86.84 \pm 0.24*
-5	96.19 \pm 1.41	94.23 \pm 0.80	93.92 \pm 0.83	82.86 \pm 0.34*
-10	99.27 \pm 1.46	94.23 \pm 0.80	94.88 \pm 0.96	78.89 \pm 0.18*
-15	103.00 \pm 0.88	94.23 \pm 0.80	94.42 \pm 1.71	74.87 \pm 0.25*
-20	107.63 \pm 0.26	94.23 \pm 0.80	74.74 \pm 7.92*	70.89 \pm 0.17*
-25	105.91 \pm 0.49	94.23 \pm 0.80	70.75 \pm 15.08*	66.89 \pm 0.26*

* $p < 0.05$.

TABLE 6. Comparison and statistical analysis of HR estimations from IMAR-reconstructed PPG for 10 different subjects (Head Experiment).

Subject	Head HR (mean \pm SD)	Finger HR (Reference) (mean \pm SD)	IMAR reconstructed HR (mean \pm SD)	ICA reconstructed HR (mean \pm SD)
1	68.31 \pm 19.25	59.23 \pm 1.49	59.76 \pm 0.22*	65.68 \pm 20.98*
2	85.39 \pm 34.53	71.55 \pm 3.037	73.72 \pm 0.31*	91.02 \pm 35.48*
3	76.19 \pm 8.88	77.39 \pm 1.360	78.705 \pm 0.33	68.06 \pm 14.14*
4	94.47 \pm 39.05	70.55 \pm 3.686	73.66 \pm 0.38*	75.32 \pm 13.42*
5	72.33 \pm 29.82	67.88 \pm 4.643	66.83 \pm 0.39	69.97 \pm 20.20*
6	45.09 \pm 10.06	51.44 \pm 1.481	49.00 \pm 0.09*	59.43 \pm 22.97*
7	44.82 \pm 24.47	59.82 \pm 1.486	57.56 \pm 0.21	64.49 \pm 35.63*
8	63.46 \pm 13.35	62.08 \pm 0.865	62.23 \pm 0.25	60.68 \pm 10.70*
9	59.37 \pm 30.85	49.05 \pm 1.555	49.19 \pm 0.20	60.27 \pm 13.24*
10	46.89 \pm 32.25	79.35 \pm 1.323	78.93 \pm 0.45	64.80 \pm 25.60*

* $p < 0.05$.**TABLE 7. Comparison and statistical analysis of SpO₂ estimations from IMAR-reconstructed PPG for 10 different subjects (Head Experiment).**

Subject	Head SpO ₂ (mean \pm SD)	Finger SpO ₂ (Reference) (mean \pm SD)	IMAR reconstructed SpO ₂ (mean \pm SD)	ICA reconstructed SpO ₂
1	82.86 \pm 4.86	97.70 \pm 0.46	97.94 \pm 0.93	76.721 \pm 38.132*
2	80.33 \pm 2.82	97.67 \pm 0.47	97.972 \pm 4.048*	111.097 \pm 1.496*
3	87.20 \pm 4.54	95.41 \pm 0.49	98.53 \pm 0.727*	74.081 \pm 21.678*
4	87.36 \pm 2.64	97 \pm 0	97.13 \pm 0.23	81.391 \pm 11.81*
5	84.25 \pm 3.76	98 \pm 0	96.82 \pm 5.25*	77.593 \pm 22.16*
6	92.38 \pm 2.64	98 \pm 0	97.47 \pm 0.97	84.069 \pm 14.84*
7	85.18 \pm 3.06	98.41 \pm 0.49	96.68 \pm 0.38	75.632 \pm 17.24*
8	90.94 \pm 2.38	99.82 \pm 0.06	97.99 \pm 0.38	89.322 \pm 17.77*
9	83.93 \pm 4.54	98 \pm 0	99.61 \pm 3.87*	100.15 \pm 16.96*
10	84.94 \pm 4.24	95.97 \pm 0.67	96.53 \pm 4.62	86.731 \pm 19.305*

* $p < 0.05$.**TABLE 8. Comparison and statistical analysis of HR estimations from IMAR-reconstructed PPG for 10 different subjects (Finger Experiment).**

Subject	Head HR (mean \pm SD)	Finger HR (Reference) (mean \pm SD)	IMAR reconstructed HR (mean \pm SD)	ICA reconstructed HR (mean \pm SD)
1	77.43 \pm 1.91	70.61 \pm 0.73	70.42 \pm 0.42	77.32 \pm 8.34*
2	63.60 \pm 2.42	78.80 \pm 0.41	78.36 \pm 0.35	79.57 \pm 9.68
3	70.82 \pm 15.01	66.18 \pm 0.76	67.21 \pm 0.26	62.96 \pm 22.53*
4	87.70 \pm 20.53	72.59 \pm 0.26	70.85 \pm 0.34	73.58 \pm 11.34*
5	84.34 \pm 4.86	74.43 \pm 0.29	73.51 \pm 0.29*	77.62 \pm 18.55*
6	81.75 \pm 6.34	67.78 \pm 0.36	69.07 \pm 0.26*	67.75 \pm 18.01
7	63.75 \pm 3.05	57.57 \pm 0.54	58.32 \pm 2.49	52.51 \pm 24.06*
8	66.75 \pm 5.03	58.27 \pm 0.75	60.34 \pm 0.44*	61.64 \pm 28.83*
9	97.27 \pm 22.74	74.39 \pm 0.46	74.25 \pm 0.68	63.60 \pm 14.96*
10	73.76 \pm 2.85	61.58 \pm 0.50	61.40 \pm 0.35	50.80 \pm 13.72*

* $p < 0.05$.

PPG Signal Reconstruction Performance in Finger Experiment

The performance of the signal reconstruction of the proposed IMAR approach is compared to TD-ICA for the PPG data with an index finger moving left-to-right patterns. The pulse oximeter on the middle finger of

the right hand, which was stationary, was used as the reference signal. Since the subjects were directed to produce the motions for 30 s within each 1-min segment, corresponding to 50% corruption by duration, the window length of both clean and corrupted segments were both set as half length of the signal.

TABLE 9. Comparison and statistical analysis of HR estimations from IMAR-reconstructed PPG for 9 different subjects (Walking & Stair Climbing Experiment).

Subject	Head HR (mean \pm SD)	Finger HR (Reference) (mean \pm SD)	IMAR reconstructed HR (mean \pm SD)	ICA reconstructed HR (mean \pm SD)
1	62.16 \pm 18.96	70.73 \pm 5.80	70.55 \pm 0.56	77.39 \pm 11.90*
2	94.30 \pm 20.37	94.40 \pm 1.69	95.54 \pm 0.86	92.94 \pm 9.99*
3	105.53 \pm 17.23	120.64 \pm 2.98	122.00 \pm 1.05	95.67 \pm 13.10*
4	95.48 \pm 8.37	101.61 \pm 3.06	99.89 \pm 0.44*	90.89 \pm 8.28*
5	82.20 \pm 13.07	86.99 \pm 3.71	87.71 \pm 1.07	82.84 \pm 17.96*
6	77.40 \pm 12.69	82.48 \pm 1.68	81.93 \pm 0.48	86.81 \pm 12.54*
7	121.02 \pm 19.26	107.58 \pm 1.51	109.15 \pm 0.07	138.62 \pm 6.18*
8	86.57 \pm 9.85	91.95 \pm 6.07	91.73 \pm 0.57	80.44 \pm 4.61*
9	87.09 \pm 6.56	82.55 \pm 5.24	84.22 \pm 1.93*	104.30 \pm 21.43*

* $p < 0.05$.**TABLE 10. Comparison and statistical analysis of SpO₂ estimations from IMAR-reconstructed PPG for 9 different subjects (Walking & Stair Climbing Experiment).**

Subject	Head SpO ₂ (mean \pm SD)	Finger SpO ₂ (Reference) (mean \pm SD)	IMAR reconstructed SpO ₂ (mean \pm SD)	ICA reconstructed SpO ₂
1	95.70 \pm 7.62	99.00 \pm 0	97.64 \pm 2.50	84.21 \pm 1.34*
2	94.55 \pm 5.51	95.37 \pm 0	96.37 \pm 0.99	95.53 \pm 1.59
3	91.00 \pm 15.58	96.75 \pm 0	94.51 \pm 0.42*	84.64 \pm 4.63*
4	89.61 \pm 3.36	99.62 \pm 0	102.25 \pm 0.65*	87.33 \pm 2.67*
5	94.27 \pm 8.12	98.00 \pm 0.50	97.34 \pm 1.45	76.50 \pm 1.53*
6	88.50 \pm 13.95	96.00 \pm 0.31	94.97 \pm 4.07*	82.94 \pm 1.05*
7	94.92 \pm 16.77	98.00 \pm 0	100.37 \pm 3.15	90.69 \pm 8.11*
8	96.11 \pm 6.60	97.00 \pm 0	98.70 \pm 4.16*	96.11 \pm 0.39
9	93.78 \pm 6.60	98.62 \pm 0	95.99 \pm 2.39*	89.11 \pm 5.03*

Table 8 compares the HR reconstruction results between the IMAR and TD-ICA methods for all 10 subjects. As shown in Table 8, the IMAR reconstructed HR values are not significantly different from the reference HR in 7 out of 10 subjects. However, the TD-ICA's reconstructed HR is significantly different from the reference HR in 8 out of 10 subjects indicating poor reconstruction fidelity.

PPG Signal Reconstruction Performance for the Walking and Stair Climbing Experimental Data

The signal reconstruction of the MNA identified data segments of the walking and stair climbing experiments using our proposed IMAR and its comparison to TD-ICA are provided in this section. Detection of the MNA data segments was performed using the algorithm described in Part I of the companion paper. The reconstructed HR and SpO₂ values using our proposed algorithm and TD-ICA are provided in Tables 9 and 10, respectively. For both HR and SpO₂ reconstruction, the measurements were carried out using PPG data recorded from the head pulse oximeter. The right hand index finger's PPG data was used as HR and SpO₂ references. As shown in Table 9,

7 out of 9 subjects' reconstructed HR values were found to be not significantly different from the reference HR values using our algorithm. While 2 subjects' reconstructed HR values were found to be significantly different than the reference, the differences in the actual HR values are minimal. For TD-ICA's reconstructed HR values, all values deviate significantly from the reference values.

For the reconstructed SpO₂ values, our algorithm again significantly outperforms TD-ICA. All but one subject are not significantly different than the SpO₂ reference values for TD-ICA. For our IMAR algorithm, only 4 out of 9 subjects do not show significant difference from the reference values. Note the zero standard deviation reference SpO₂ values from Massimo's pulse oximeter in 7 out of 9 subjects. This is because Massimo uses a proprietary averaging scheme based on several past values. Hence, it is possible that the significant difference seen with our algorithm in some of the subjects would turn out to be not significant if the averaging scheme were not used. While some of the SpO₂ values from our algorithm are significantly different from the reference, the actual deviations are minimal and they are far less than with TD-ICA.

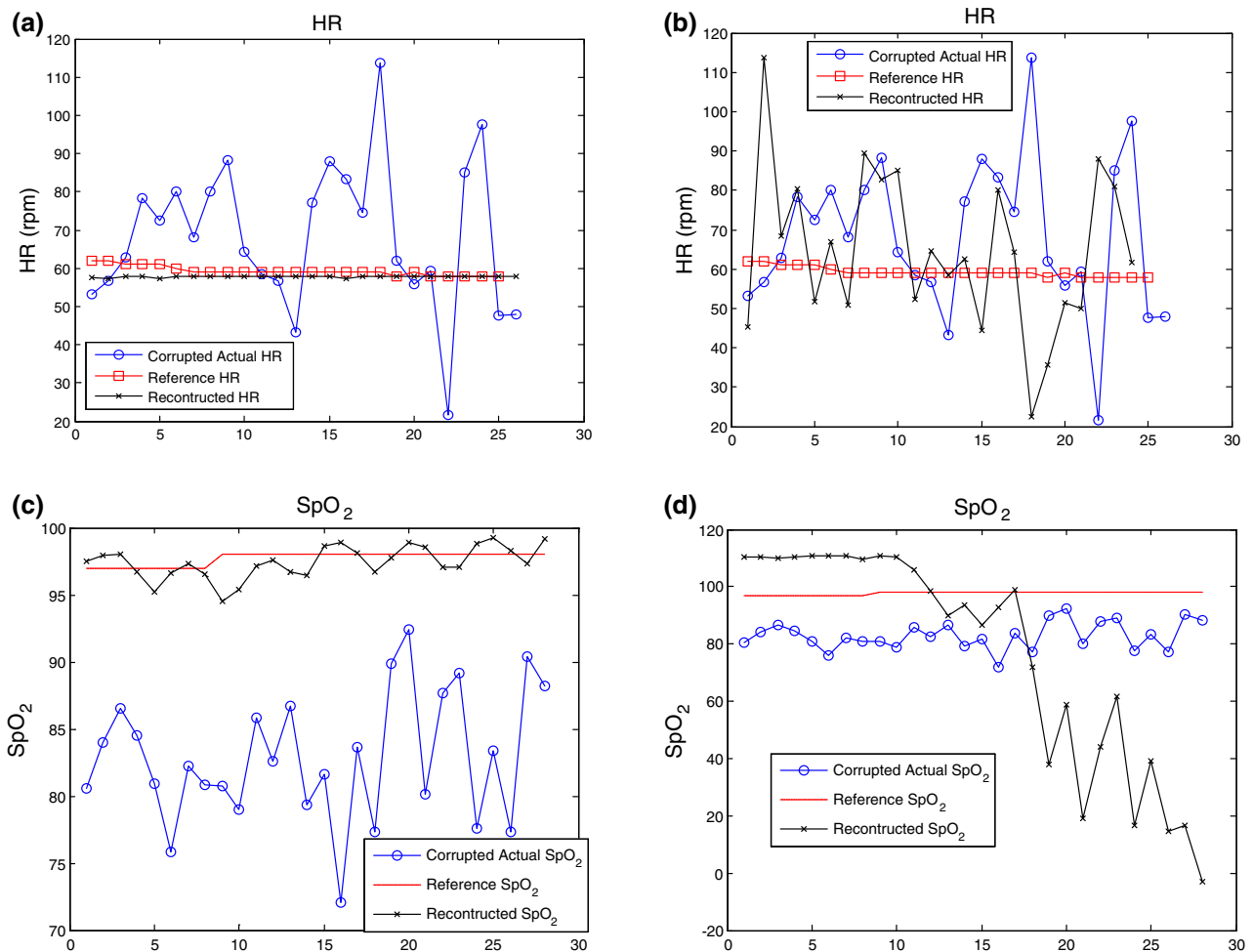


FIGURE 4. (a) HR estimated from IMAR-reconstructed PPG compared to reference and corrupted PPG; (b) HR estimated from ICA-reconstructed PPG compared to reference and corrupted PPG; (c) SpO₂ estimated from IMAR-reconstructed PPG compared to reference and corrupted PPG; (d) SpO₂ estimated from ICA-reconstructed PPG compared to reference and corrupted PPG.

DISCUSSION

In this study, a novel IMAR method is introduced to reconstruct MNA contaminated segments of PPG data. Detection of MNA using a support vector machine algorithm was introduced in the companion paper. The aim of the current paper is to reconstruct the MNA corrupted segments as closely as possible to the non-corrupted data so that accurate HRs and SpO₂ values can be derived. The question is how to reconstruct the MNA data segments when there is no reference signal. To address this question, we use the most adjacent prior clean data segment and use its dynamics to derive the MNA contaminated segment's HRs and oxygen saturation values. Hence, the key assumption with our IMAR technique is that signal's dynamics do not change abruptly between the MNA contaminated segment and its most adjacent prior clean portion of data. Clearly, if this assumption is violated, the IMAR's ability to reconstruct the dynamics of the sig-

nal will be compromised. We are currently working on a time-varying IMAR algorithm to address this issue.

There are hosts of algorithms available for MNA elimination and signal reconstruction. Various adaptive filter approaches to remove MNA have been proposed with good results but the test data to fully evaluate the algorithms are either limited or confined to laboratory controlled MNA involving simple finger or arm movements.^{11,19,24,25} Moreover, these adaptive filter methods work best when a reference signal is available.

For those methods that do not require a reference signal to remove MNA, there have been many algorithms developed based on variants of the ICA.^{16,18,21,25} Most of the ICA-based methods produced reasonably good signal reconstructions of the MNA contaminated data. However, most of these methods were validated on data that were collected using laboratory controlled MNA involving pre-de-

fined simple side-to-side or up-and-down finger and arm movements.^{16,18,21,25}

Given that ICA-based methods produced good signal reconstructions of the MNA contaminated data, we have compared our proposed approach to the TD-ICA method as described by Krishnan *et al.*¹⁸ using simulated data, laboratory controlled data as well as daily activity data involving both walking and stair climbing movements. Krishnan *et al.* proposed frequency-domain ICA and compared its performance to the TD-ICA but the improvement is marginal at the expense of higher computational complexity, hence, we used the latter method. Comparison of the performance of our method to TD-ICA was based on reconstruction of HR and SpO₂ values since these measures are currently used by clinicians.

Comparing HR and SpO₂ estimations of the reconstructed signal to the reference measurements using both simulation and experimental data have shown that the proposed IMAR method is a promising tool as the reconstructed values were found to be accurate. The simulation results from noise sensitivity analysis showed that SNR level down to -20 and -15 dB from additive white and colored noise, respectively, can be tolerated well by the application of the proposed IMAR procedure, compared to the SNR values of -10 and -15 dB for the TD-ICA method. Application of the proposed IMAR approach and the TD-ICA to three different sets of experimental data have also shown significantly better signal reconstruction performance with our IMAR algorithm. It is our opinion that ICA is not a good approach for signal reconstruction because its performance suffers from arbitrary scaling and random gain changes in the output signal; these would detrimentally affect the accuracy of SpO₂ estimates.

The use of singular spectrum analysis (SSA) to a single channel EEG recordings to extract high amplitude and low frequency MNA has been previously performed.²⁶ The main aim of the work by Teixeira *et al.* was to remove the artifacts in EEG signals, hence, an iterative approach to reconstruct the main dynamics of the signal was not implemented. The novelty of our approach is based on the use of SSA combined with an iterative approach to reconstruct the portion of the MNA contaminated data with the most likely true dynamics (i.e., non-MNA contaminated data) of the pulse oximeter signal. In summary, the advantages of the IMAR algorithm is that it can obtain accurate frequency dynamics and amplitude estimates of the signal, hence, the reconstructed HR and SpO₂ estimates should not deviate much from the true uncorrupted values. The disadvantage of the IMAR algorithm is that because it is an iterative approach, the computational complexity is high, hence, in the current form, it is most suitable for offline data ana-

lysis. We are not aware of any previous applications of SSA-based algorithms for MNA reconstruction of pulse oximeter data. In conclusion, a scenario where a reference signal is not available to remove the MNA, the proposed IMAR algorithm is a promising new approach to accurately reconstruct HR and SpO₂ values from MNA contaminated data segments.

ACKNOWLEDGMENTS

This work was supported in part by the US Army Medical Research and Materiel Command (USAMRMC) under Grant No. W81XWH-12-1-0541.

REFERENCES

- ¹Bishop, G and G. Welch. An Introduction to the Kalman Filter. Tech. Rep, 2006.
- ²Choi, S., A. Cichocki, H. Min Park, and S. Young Lee. Blind source separation and independent component analysis: a review. *Neural Inf. Process. Lett. Rev.* 6:1–57, 2004.
- ³Chon, K. H., S. Dash, and K. Ju. Estimation of respiratory rate from photoplethysmogram data using time-frequency spectral estimation. *IEEE Trans. Bio-med. Eng.* 56:2054–2063, 2009.
- ⁴Comon, Pierre. Independent component analysis, a new concept? *Signal Process.* 36:287–314, 1994.
- ⁵Diniz, P. Adaptive Filtering: Algorithms and Practical Implementation. Berlin: Springer Science, Business Media L.L.C., 2008.
- ⁶Elsner, J. B., and A. A. Tsonis. Singular Spectrum Analysis: A New Tool in Time Series Analysis. Berlin: Springer, 1996.
- ⁷Feleppa, J., and E. J. Mamou. Singular spectrum analysis applied to ultrasonic detection and imaging of brachytherapy seeds. *Acoust. Soc. Am.* 21:1790–1801, 2007.
- ⁸Gao, J., C. Zheng, P. Wang. Online removal of muscle artifact from electroencephalogram signals based on canonical correlation analysis. *Clin. EEG Neurosci.* 41(1):53–59, 2010.
- ⁹Ghaderi, F., H. R. Mohseni, and S. Sanei. Localizing heart sounds in respiratory signals using singular spectrum analysis. *IEEE Trans. Biomed. Eng.* 58:3360–3367, 2011.
- ¹⁰Golyandina, N., V. Nekrutkin, and A. A. Zhigljavsky. Analysis of Time Series Structure: SSA and Related Techniques. London: Taylor & Francis, 2001.
- ¹¹Hamilton, P. S., M. G. Curley, R. M. Aimi, *et al.* Comparison of methods for adaptive removal of motion artifact. In: *Computers in Cardiology 2000*, pp. 383–386, 2000.
- ¹²Hassani, H. Singular spectrum analysis: methodology and comparison. *J. Data Sci.* 5:239–257, 2007.
- ¹³Jolliffe, I. T. Principal Component Analysis. Berlin: Springer, 1986.
- ¹⁴Jubran A. Pulse oximetry. In: *Applied Physiology in Intensive Care Medicine*, edited by G. Hedenstierna, J. Mancebo, L. Brochard, *et al.* Berlin: Springer, pp. 45–48.
- ¹⁵Kalman, R. E. A new approach to linear filtering and prediction problems transactions of the ASME. *J. Basic Eng. Ser. D* 1:2, 1960.

- ¹⁶Kim, B. S., and S. K. Yoo. Motion artifact reduction in photoplethysmography using independent component analysis. *IEEE Trans. Biomed. Eng.* 53:566–568, 2006.
- ¹⁷Kloeden, P. E., and E. Platen. Numerical Solution of Stochastic Differential Equations. Berlin: Springer, 1992.
- ¹⁸Krishnan, R., B. Natarajan, and S. Warren. Two-stage approach for detection and reduction of motion artifacts in photoplethysmographic data. *IEEE Trans. Biomed. Eng.* 57:1867–1876, 2010.
- ¹⁹Morbidi, F., A. Garulli, D. Prattichizzo, *et al.* Application of Kalman filter to remove TMS-induced artifacts from EEG recordings. *IEEE Trans. Control Syst. Technol.* 16:1360–1366, 2008.
- ²⁰Ram, M. R., K. V. Madhav, E. H. Krishna *et al.* Use of multi-scale principal component analysis for motion artifact reduction of PPG signals. Recent Advances in Intelligent Computational Systems (RAICS), 2011 IEEE. pp. 425–430, 2011.
- ²¹Ram, M. R., K. V. Madhav, E. H. Krishna, *et al.* ICA-based improved DTCWT technique for MA reduction in PPG signals with restored respiratory information. *IEEE Trans. Instrum. Meas.* 62:2639–2651, 2013.
- ²²Reddy, K. A., B. George, N. Madhu Mohan *et al.* A novel method of measurement of oxygen saturation in arterial blood. Instrumentation and Measurement Technology Conference Proceedings, 2008 IMTC 2008 IEEE, pp. 1627–1630, 2008.
- ²³Reddy, K. A., B. George, N. M. Mohan, *et al.* A novel calibration-free method of measurement of oxygen saturation in arterial blood. *IEEE Trans. Instrum. Meas.* 58:1699–1705, 2009.
- ²⁴Syedtabaai, S. and L. Syedtabaai. Kalman Filter Based Adaptive Reduction of Motion Artifact from Photoplethysmographic Signal, Vol. 37. World Academy of Science, Engineering and Technology, 2008.
- ²⁵Sweeney, K. T., T. E. Ward, and S. F. Mcloone. Artifact removal in physiological signals—practices and possibilities. *IEEE Trans. Inf. Technol. Biomed.* 16:488–500, 2012.
- ²⁶Teixeira, A. R., A. M. Tomé, E. W. Lang, *et al.* Automatic removal of high-amplitude artefacts from single-channel electroencephalograms. *Comput. Methods Programs Biomed.* 83:125–138, 2006.
- ²⁷Thakor, N. V., and Y.-S. Zhu. Applications of adaptive filtering to ECG analysis: noise cancellation and arrhythmia detection. *IEEE Trans. Biomed. Eng.* 38:785–794, 1991.
- ²⁸Thompson, B. Canonical Correlation Analysis: Uses and Interpretation. Thousand Oaks: SAGE Publications, 1984.